Journal of Materials Chemistry

Cite this: J. Mater. Chem., 2012, 22, 13773

www.rsc.org/materials

PAPER

The use of a glucose-reduced graphene oxide suspension for photothermal cancer therapy†

Omid Akhavan,*[ab] Elham Ghaderi,[a] Samira Aghayee,[a] Yasamin Fereydooni[a] and Ali Talebi[a]

Received 6th March 2012, Accepted 30th April 2012
DOI: 10.1039/c2jm31396k

A single-step green method for effective reduction and functionalization of graphene oxide (GO) by glucose was developed. Then, efficacy of the glucose-reduced GO sheets in photothermal therapy of LNCaP prostate cancer cells was investigated *in vitro*. The GO suspension reduced and functionalized by glucose in the presence of Fe catalyst showed a biocompatible property with an excellent near-infrared (NIR) photothermal therapy efficiency better than hydrazine-reduced GO, single-wall and multi-wall carbon nanotube suspensions which even showed some levels of toxicities. For complete destruction of the cancer cells at some time intervals of NIR irradiation (*e.g.*, 0.5 and 12 min with a power density of 7.5 W cm^{-2}), minimum concentrations of the reduced GO sheets (*i.e.*, 1 and 0.05 mg mL^{-1}) were obtained. The high photothermal therapy efficiency and biocompatibility of the glucose-reduced GO sheets were assigned to functionalization of the reduced sheets by gluconate ions which also prevented their aggregation. Our results suggest that the glucose-reduced GO sheets can be used as biocompatible and efficient photothermal agents in upcoming nanotechnology-based cancer therapies without any common functionalization by polyethylene glycol.

1. Introduction

Although valuable techniques (such as surgery, chemotherapy, radiotherapy, and sometimes a combination of them) have been developed in the area of cancer therapies, there are still important obstacles (*e.g.*, severe adverse reactions[1,2] and low efficiency *versus* resistant cancer cells[3,4]) which should be resolved. In recent years, photothermal nanotherapy has been proposed for effective treatment of advanced-stage cancer, with low side effects.[5–7] It relies on heat generation in a nanomaterial upon near-infrared (NIR) photoexcitation and destroying cancer cells by excessive local heating.

Graphene (as a monolayer or a few layers of sp^2-bonded carbon atoms having a honeycomb lattice structure) with unique physicochemical properties (*e.g.*, see ref. 8) has attracted much attention. Furthermore, being very similar to carbon nanotubes (CNTs), graphene is capable of absorbing NIR radiation, because of its delocalized electron arrangement. This absorbed radiation can be given off to vibrational modes of the graphene *i.e.*, transformation into thermal energy, which results in raising the temperature of the cancerous tissue and structural changes in the cellular and protein configurations.[9] Hence, graphene sheets with an excellent thermal conductivity[10] and a high effective surface area (as the thinnest sheet) can be considered as one of the most effective nanomaterials in photothermal nanotherapy applications.

So far, only a few works about photothermal therapy of cancer cells by graphene-based nanomaterials have been reported. For example, for the first time, Yang *et al.*[11] studied photothermal therapy of cancer cells *in vivo*, by using nanoscale graphene oxide (nGO) sheets coated by polyethylene glycol (PEG). Then, the effect of surface chemistry and size of nanoscale graphene oxide sheets on cancer photothermal therapy using ultra-low laser power was reported by this group.[12] Robinson *et al.*[13] studied photothermal therapy of cancer cells *in vitro*, by using a low concentration of nanoscale reduced graphene oxide (nRGO)-PEG. Zhang *et al.*[14] reported the synergistic effect of chemo-photothermal therapy using PEGylated graphene oxide. And Markovic *et al.*[15] found that polyvinylpyrrolidone-coated graphene nanoparticles show better performance in photothermal therapy of cancer cells *in vitro* than DNA or sodium dodecylbenzenesulfonate-solubilized single-wall carbon nanotubes (SWCNTs). In most of these recent works, in order to overcome the water-insolubility of hydrazine-reduced graphene oxide sheets, functionalization by PEG was used. In addition, PEG-functionalized nRGO sheets exhibited a biocompatible property, while nGO and nRGO appeared to show similar levels of toxicity.[13]

In fact, biocompatibility of graphene-based nanomaterials is one of the most important parameters for their applications in (especially *in vivo*) photothermal therapy of cancer cells.

[a]*Department of Physics, Sharif University of Technology, P.O. Box 11155–9161, Tehran, Iran. E-mail: oakhavan@sharif.edu; Fax: +98–21–66164566; Tel: +98–21–66164566*
[b]*Institute for Nanoscience and Nanotechnology, Sharif University of Technology, P.O. Box 14588–89694, Tehran, Iran*
† Electronic supplementary information (ESI) available. See DOI: 10.1039/c2jm31396k

Although, there are some investigations about biocompatibility of graphene,[16] interaction of extremely sharp edges of graphene sheets with cell wall membrane,[17] generation of reactive oxygen species by graphene[18] and trapping a live cell within the aggregated graphene sheets[19] were reported as possible mechanisms for describing the cytotoxicity of graphene sheets. It was also reported that the graphene-based papers can inhibit the growth of bacteria but with a minimal cytotoxicity.[20] Cytotoxicity of graphene is also reported to be dose dependent.[18,21] Moreover, in the chemical exfoliation method (as one of the most efficient methods for large scale production of graphene), strong reductants such as hydrazine, which is highly toxic, are usually applied for reduction of the synthesized graphene oxide suspensions. Therefore, not only should a biocompatible reductant be selected and used for reduction of the chemically exfoliated GO suspensions (*e.g.*, melatonin,[19,22] vitamin C (L-ascorbic acid),[23] sugar,[24] polyphenols of green tea[25] and bacteria[26,27]), but biocompatibility of the reduced graphene oxide suspension must also be tested for a noninvasive and harmless application of graphene-based nanomaterials in photothermal therapy. In addition, lower amounts and concentrations of graphene with higher NIR absorbance and heat transport efficiencies should be prepared and utilized for the photothermal therapy. One of the ways for achieving this is prevention from aggregation of reduced graphene oxide sheets during the biocompatible reduction process at the neutral pH.

In this work, at first, we used glucose for green reduction and functionalization of graphene oxide sheets synthesized through a chemical exfoliation method. The efficiency of reduction by glucose in the presence of a Fe catalyst was investigated. The biocompatibility of the glucose-reduced graphene oxide was examined and compared to the biocompatibility of hydrazine-reduced graphene oxide, without using any PEGylation which is usually applied for functionalization of the reduced sheets. Then, the biocompatible glucose-reduced graphene oxide suspension was used for NIR photothermal therapy of human prostate cancer cells *in vitro*. For some various NIR irradiation times, the minimum GO concentration required for complete lysis of the cancer cells was obtained. Efficiency and biocompatibility of the graphene-based nanomaterials in photothermal therapy were also compared with those of single-wall carbon nanotubes and multi-wall carbon nanotubes (MWCNTs).

2. Experimental method

2.1. Synthesis of graphene oxide (GO)

Natural graphite powder (particle diameter of $\leq$20 μm, Fluka) was utilized as the raw material to prepare graphite oxide suspension through an improved Hummers' method. The details of this method were previously reported elsewhere.[22] The prepared graphite oxide powder was dispersed in deionized (DI) water to obtain an aqueous graphite oxide suspension with a yellow-brownish color. The suspension was centrifuged at 2000 rpm for 15 min to eliminate unexfoliated graphitic plates and then at 8000 rpm for 10 min to remove tiny graphite particles. Finally, GO suspension was achieved by exfoliation of the filtered graphite oxide suspension through its sonication at a frequency of 40 kHz and power of 150 watt for 1 h.

2.2. Reduction of graphene oxide by glucose

To obtain GO suspension reduced by glucose in the presence of Fe catalyst (GRGO-Fe), at first, 160 μL glucose solution ($C_6H_{12}O_6$, dextrose 50%) was added to 10 mL of the prepared GO suspension with a concentration of 0.1 mg mL^{-1} and pH $\approx$ 7, at room temperature. Then, by using a magneto-stirrer heater, the glucose-GO suspension was stirred at 400 rpm at a temperature of 95 °C in the presence of a Fe foil with dimensions of 10 mm $\times$ 10 mm $\times$ 1 mm in air for 30 min. The glucose-reduced GO (GRGO) suspension was obtained by the same procedure, but without applying the Fe catalyst. To have a better comparison, the efficacy of the glucose solution for reduction of the GO suspension in the presence of the Fe catalyst was compared to the efficacies of hydrazine (with a concentration of 5 mM) at 90 °C for 10 min. To prevent the fast aggregation of the reduced GO, pH of the hydrazine-reduced GO (HRGO) suspension was adjusted to the range of 9–10 by using ammonia solution ($\sim$2 μL for each mL of the suspension).

To compare the photothermal efficiency of our graphene based materials with the efficiency of carbon nanotubes (CNTs), SWCNT (HiPco, with residual Fe catalyst <35 wt%, diameter of 0.8–1.2 nm and length of $\sim$100 to 1000 nm) and MWCNT (with purity of 95%, outer diameter of 10–30 nm and length of <5–15 μm,[28,29] provided from io.li.tec) powders were used. To obtain homogeneous suspension, the CNTs were chemically functionalized by sonicating in nitric acid (65%, Merck) at 60–70 °C. Then, the functionalized CNTs were filtered and washed with DI water. Finally, a desired amount of the functionalized CNT powders were dispersed uniformly in DI water.

2.3. Material characterization

The surface topography and height profile of the GO and reduced-GO layers were studied by using atomic force microscopy (AFM, Digital Instruments NanoScope V) in tapping mode. The coatings for the AFM imaging were prepared by drop-casting a diluted suspension (0.01 mg mL^{-1}) onto a cleaned Si(100) substrate. A UV-vis spectrophotometer (PerkinElmer UV-Vis-NIR Model Lambda 950) was used to investigate the optical absorption of the GO and the reduced GO suspensions in the wavelength range of 200–1000 nm. X-ray photoelectron spectroscopy (XPS) was utilized to examine chemical states of the GO layers under the different reducing conditions. The data were obtained through a hemispherical analyzer equipped by an Al Kα X-ray source ($h\nu$ = 1486.6 eV) operating under a vacuum <10^{-7} Pa. The XPS peaks were deconvoluted by using Gaussian components after a Shirley background subtraction. To study the carbon structure of the samples, Raman spectroscopy (HR-800 Jobin-Yvon) using an Nd–YAG laser source operating at a wavelength of 532 nm was applied at room temperature.

2.4. Cell culture and cellular incubation in graphene-based suspension

The human prostate cancer cell line LNCaP (ATCC, Rockville, MD) was cultured in RPMI-1640 medium (ATCC, Rockville, MD) supplemented with 10% fetal bovine serum (FBS) and 1% penicillin–streptomycin. Then, the cancer cells were incubated within a 100 mL flask containing $\sim$2 $\times$ 10^6 cells and 200 μL

reduced GO suspension (with various concentrations of GO ranging from 0.001 to 1 mg mL^{-1}) for 24 h at 37 °C in a 5% CO_2 atmosphere. As an advantage, no significant aggregation was observed for the GRGO and GRGO-Fe added to the culture medium, while the GO suspension showed a slight instability in the culture medium.

2.5. Photothermal therapy and determination of live cells

For NIR photothermal therapy, the cancer cells incubated in the graphene-based suspension were transferred to a cubic quartz cuvette (with dimension of 2 cm) and exposed to an 808 nm diode laser source (JENOPTIK unique-mode GmbH, Germany) with the beam diameter of about 1 cm and power density of 7.5 W cm^{-2}. After the photothermal process, the number of live cells was determined using a 3-(4,5-dimethylthiazol-2-yl)-2,5-diphenyltetrazolium bromide (MTT) cell proliferation assay kit. The data reported in this work are the average of three measurements. To have some optical images from the photothermal destruction of the cells, multiple regions of the GRGO-incubated cancer cells cultured on a plate were exposed to the NIR laser irradiation for various periods of time and then stained with 1% Trypan Blue for 15 min to check the cell viability. A dead cell absorbs the dye and shows a blue color cell, while a living cell eliminates the dye and stays transparent.

2.6. Measurement of heating of the graphene-based suspensions by NIR irradiation

The graphene-based suspensions were heated under irradiation by the NIR laser. Temperature of the suspensions was measured at 15 s intervals with a thermocouple located inside the suspension for a total time of 2 min. In order to minimize the direct heating, exposure of the thermocouple by the laser beam was prevented.

3. Results and discussion

Fig. 1a presents AFM images of the GO sheets deposited on the Si substrate. Three overlapped sheets are observable in the image. The height profile diagram of the AFM image indicates that the thickness of the sheets is around 1 nm, comparable to the typical thickness of the single-layer GO sheets (~0.8 nm).[30,31] Fig. 1b shows the GO sheets reduced by hydrazine with an average thickness of ~0.55 nm. In fact, removing the epoxy and hydroxyl groups from both sides of GO sheets results in ~0.44 nm decrease, approaching the thickness of graphene (~0.36 nm).[32] Fig. 1c exhibits the GO sheets reduced by glucose in the presence of Fe catalyst with an average thickness of ~1.4 nm. The increase in thickness of the reduced sheets (~1 nm) can be assigned to adsorption of reductant molecules (here, glucose-based molecules) on both sides of the reduced sheets, as reported by Su *et al.*,[33] but for some aromatic molecules. Then, the remaining thickness of about 0.4 nm can be attributed to the thickness of the reduced GO sheets, as similarly reported for GO sheets reduced by vitamin C[23] and melatonin.[22]

The optical absorption spectra of the GO and reduced GO suspensions are exhibited in Fig. 2. After reduction of the GO by either glucose or hydrazine, the color of the GO suspension changed from light brown to black (see the inset of Fig. 2). The

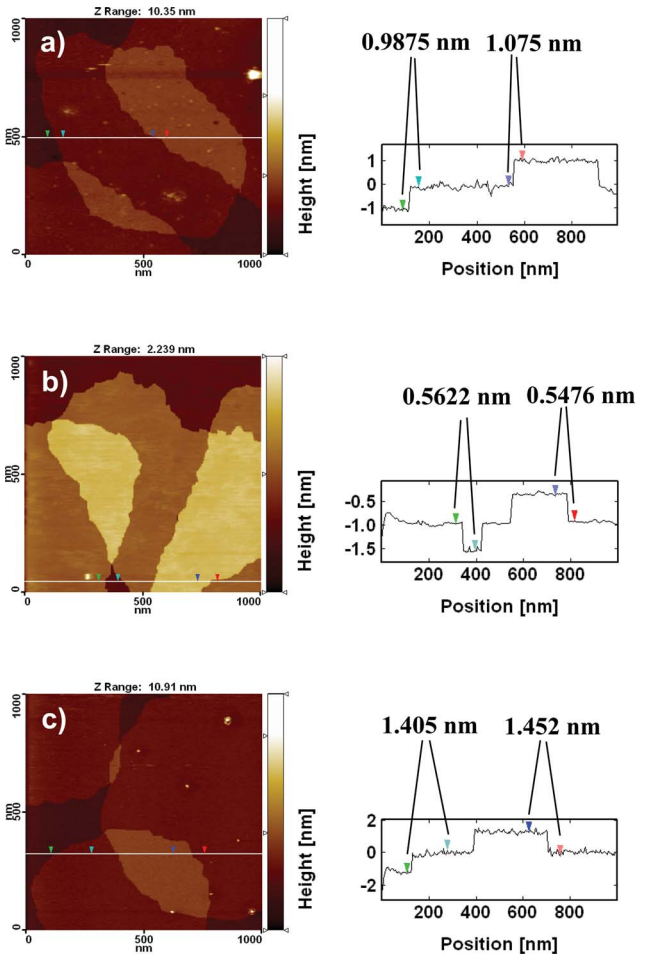

Fig. 1 AFM images of (a) the GO nanosheets and the GO nanosheets reduced by (b) hydrazine at 90 °C for 10 min and (c) glucose in the presence of a Fe foil catalyst at 95 °C for 30 min. Vertical distances of the markers were noted above the height profile diagrams.

black color of the reduced GO suspensions can be assigned to partial restoration of the π network between the sheets due to removing the oxygen-containing bonds resulting in electronic

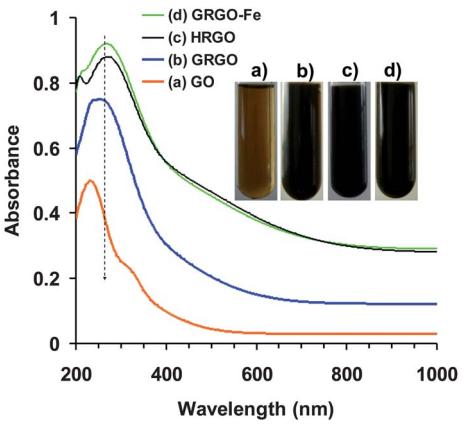

Fig. 2 UV-vis absorption spectra of (a) GO, (b) GRGO, (c) HRGO, and (d) GRGO-Fe suspensions with GO concentration of 0.5 mg mL^{-1}. Inset shows digital pictures of the reduced GO suspensions (b–d) as compared to the as-prepared GO suspension (a).

conjugation within reduced sheets.[34] The optical absorption spectra also show that the absorption peak of the GO suspension is around 228 nm, while the absorption peaks of the reduced suspensions shift into wavelengths of around 265 nm, corresponding to deoxygenation of the GO suspension under the reduction processes. It is also seen that the absorption around wavelength of 800 nm significantly increased by reduction of the GO suspension. The GO reduced by hydrazine and glucose in the presence of Fe showed the highest optical absorption among the samples. The lower optical absorption of the GRGO sample can be assigned to incomplete reduction of the GRGO as compared to the reduction of the HRGO and GRGO-Fe suspensions.

To study the effect of glucose on the deoxygenation of the GO suspension in more detail, XPS was used. Fig. 3 shows deconvoluted C (1s) peaks of the GO reduced by glucose in the absence and in the presence of Fe catalyst, as compared to the peaks of the as-prepared GO and the HRGO. The deconvoluted peak centered at 285.0 eV was attributed to the C–C and C=C bonds. The other peaks located at the binding energies of 286.5, 287.2, 288.2 and 289.4 eV were attributed to the C–OH, C–O–C, C=O, and O=C–OH oxygen-containing functional groups, respectively (see, *e.g.*, ref. 35 and 36). In order to quantitatively investigate the chemical states of the GO sheets at the various reduction conditions, the peak area ratios of the C–OH, C–O–C, C=O and O=C–OH peaks to the CC peak were extracted from the deconvoluted peaks, as given in Table 1. It was found that glucose is able to partially reduce the GO (compare Fig. 3a and b), but the reduction level of the GO by glucose in presence of the Fe catalyst (Fig. 3d) was comparable to the reduction level

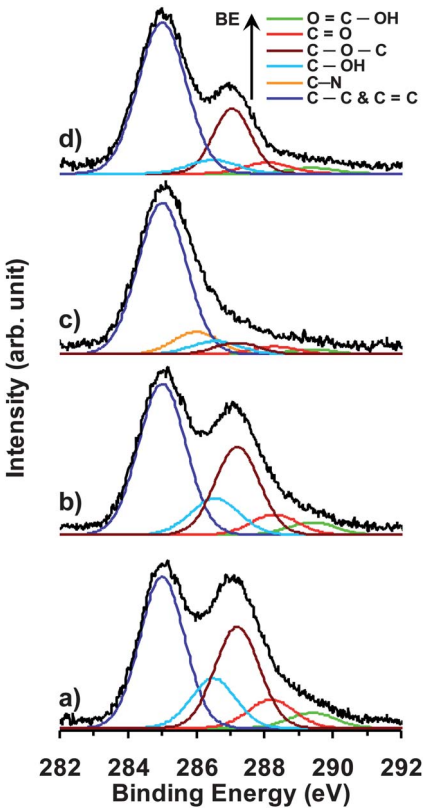

Fig. 3 Peak deconvolution of C (1s) core level of XPS spectra of (a) GO, (b) GRGO, (c) HRGO and (d) GRGO-Fe.

Table 1 The peak area (A) ratios of the oxygen-containing bonds to the CC bonds and the peak intensity ratio of I_D/I_G of the GO reduced in the various conditions

			GO reduced by		
Samples		GO	Glucose	Hydrazine	Glucose-Fe
XPS	A_{CN}/A_{CC}	—	—	0.14	—
	A_{COH}/A_{CC}	0.33	0.25	0.08	0.09
	A_{COC}/A_{CC}	0.67	0.55	0.07	0.33
	A_{CO}/A_{CC}	0.19	0.13	0.05	0.07
	A_{OCOH}/A_{CC}	0.11	0.08	—	0.04
Raman	I_D/I_G	1.22	1.18	1.37	0.97

achieved by hydrazine (Fig. 3e), except that the XPS of the HRGO indicated another peak component at 286.0 eV relating to formation of a C–N bond (see, for example, ref. 22). In addition, although no peak relating to formation of the C–N bond was observed in the XPS of the GO reduced by glucose, the XPS peak of the GRGO-Fe exhibited a significant deconvoluted peak relating to epoxide groups. The presence of epoxide groups in the reduced sample was assigned to functionalization of the reduced sheets through formation of a chemical bond between the gluconate ions and the carbons of the reduced GO, as discussed further in the following paragraphs. The quantitative variations in the chemical state of the GO after the reduction processes are given in Table 1. It is worth noting that the Fe (2p) core level of the Fe catalyst before use in the reduction process was consistent with the Fe^0 chemical state and no significant change was observed after the reduction process by glucose. This confirmed that the Fe foil did not oxidize and acted as a catalyst during the reduction process.

Raman spectroscopy is known as an effective technique for investigation of the single- and multi-layer properties of graphene sheets. Here, the effects of the various reduction conditions on the Raman characteristics of the reduced GO sheets were examined, as shown in Fig. 4. The famous properties of carbon materials in Raman spectra are the G band (~1580 cm^{-1}) originated from the phonon scattering of the graphitic structure and the D band (~1350 cm^{-1}) relating to formation of sp^3 defect bonds caused by

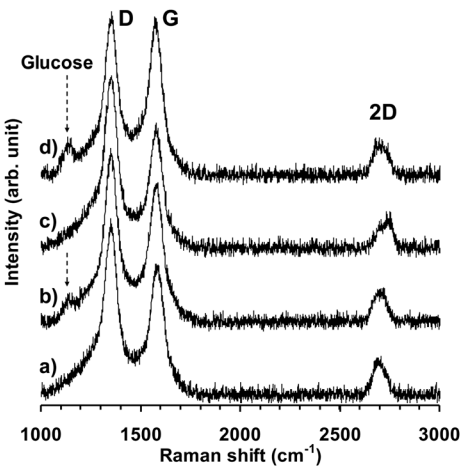

Fig. 4 Raman spectra of (a) GO, (b) GRGO, (c) HRGO and (d) GRGO-Fe.

oxidation.[37,38] In addition, the D band can result from vacancies, grain boundaries, edge defects and amorphous carbon species in a disordered carbon structure.[39] In this regard, the I_G/I_D ratio is defined as a parameter for measuring the sp^2 domain size of a carbon structure containing sp^3 and sp^2 bonds. In this work, for the GO suspensions reduced at the different conditions, the I_D/I_G ratios (inverse of I_G/I_D) were given in Table 1. It was found that deoxygenation of the GO sheets by using glucose solution in the presence of the Fe catalyst resulted in reduction of the I_D/I_G ratio which can be attributed to recovering the graphitic structure of the GO sheets during the reduction. However, for the HRGO the I_D/I_G ratio was found to be about 1.37 which can be assigned to an increase in the defects on the surface of the reduced GO through formation of the C–N bonds.

Raman spectra of graphene-based materials also show a 2D band (described by the adopted double resonant model[39,40]) which is sensitive to stacking of graphene sheets.[41] For single-layer graphene sheets, the 2D band generally appears as a Lorentzian peak centered at 2679 cm^{-1}, while for multilayer graphene sheets (including 2–4 layers) the 2D band shows a wider peak with 19 cm^{-1} shift to higher wavenumbers.[42] Fig. 4 shows that the 2D band of the as-prepared GO sheets centered about 2686 cm^{-1} with a low-intensity shoulder at the higher wavenumbers. Hence, monolayer GO sheets were present in the as-prepared GO suspension. Although, the 2D bands of the HRGO exhibited a significant shift into the higher wavenumbers, the 2D band of the GRGO-Fe showed only a slight shift indicating lower aggregation of the GO sheets reduced by glucose in the presence of the Fe catalyst. The lower aggregation in the GRGO-Fe suspension can be assigned to adsorption of the gluconate ions on the reduced sheets, consistent with the results obtained by the XPS analysis. Furthermore, the peak appearing at ~1130 cm^{-1} confirmed attachment of glucose and/or glucose oxide molecules on the surface of the GRGO-Fe sheets (see Fig. 4d). On the other hand, the lower aggregation in the GRGO suspension (as resulted from the lower shift in the 2D band) can be assigned to its lower reduction level. Meanwhile, the Raman spectrum (Fig. 4b) shows lower amounts of glucose and/or glucose oxide molecules on the surface of the GRGO sheets.

It was shown that metallic particles such as Au, Pt and Pd[36] and metal oxides such as TiO_2,[43–45] ZnO[46–48] and WO_3 (ref. 49 and 50) can play a (photo)catalytic role in the reduction of graphene oxide, through electron transfer from (photo)catalysts into graphene oxide. Here, the Fe foil can play the same role as catalyst and contribute the electrons transferred into the GO based on the following reactions:

$$Fe \rightarrow Fe^{2+} + 2e^-$$

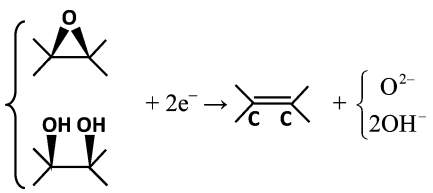

in which the upper and lower symbols show epoxide and hydroxide of GO, respectively. Now, the Fe^{2+} can promote oxidation of the glucose in the presence of oxygen dissolved in the aqueous solution as shown in the following:[51]

$$\text{Glucose } (C_6H_{12}O_6) + H_2O + Fe^{2+} \rightarrow \text{Gluconic acid } (C_6H_{12}O_7) + Fe + 2H^+$$

Then, the glucose oxidation results in reduction of GO as follows:

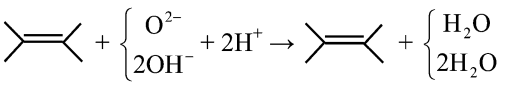

In addition, glucose and gluconic acid can chemically bond to carbon of GO as schematically shown in Fig. 5 for glucose. This bonding is similar to chemical bonding of glucose to phosphate groups through phosphorylation of glucose which was previously reported by others (see, for example, ref. 52). The steric effect of this chemical bonding (for which formation of its C–O–C bond on the surface of the reduced GO sheet was confirmed by the XPS analysis of the GRGO-Fe) resulted in low aggregation of the reduced GO sheets, as also found by Raman analysis.

The GRGO-Fe sheets which were obtained by using a green reaction were utilized for destruction of LNCaP prostate cancer cells through a photothermal therapy. After the therapy, cell viability of the cancer cells was detected by MTT test. The photothermal effects of GRGO-Fe and also other graphene-based materials (*i.e.*, GO, GRGO, and HRGO) on the therapy of

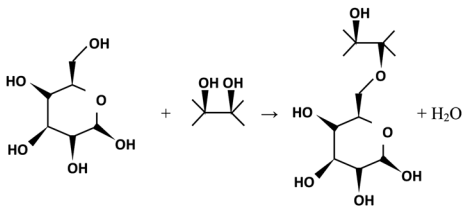

Fig. 5 Schematic reaction of glucose and hydroxyl bonds of GO.

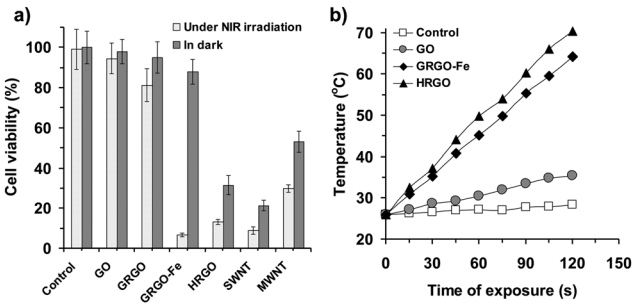

Fig. 6 (a) Cell viability of LNCaP prostate cancer cells after exposure to the GO suspension and the GRGO, GRGO-Fe, and HRGO with GO concentration of 0.1 mg mL^{-1}, as compared to the same concentration for the oxidized SWCNTs and MWCNTs, under irradiation of an 808 nm laser source with power density of 7.5 W cm^{-2} for 1 min and in the dark for 24 h. Control sample shows the cell viability in a solution without any GO additive. (b) Temperature evolution of the cancer cell solution containing 0.1 mg mL^{-1} of the GO, GRGO-Fe and HRGO during continuous irradiation by the laser source for 2 min.

the cancer cells were investigated and compared to the corresponding effects of the oxidized SWCNT and MWCNT powders as benchmarks for carbon nanomaterials. Concerning this, Fig. 6a shows that by using GRGO–Fe, HRGO, SWCNT and MWCNT suspensions most of the cancer cells (~93, 87, 91 and 70%) died just after 1 min, while using the GRGO only ~18% of the cells were destroyed at the same irradiation time. The GO suspension was transparent and so no significant cancer cell destruction was observed, very similar to the control sample with no carbon nanomaterials.

Because a portion of the observed cell destruction can be assigned to cytotoxicity of the carbon nanomaterials, we also checked MTT cytotoxicity of our carbon-based nanomaterials in the dark, as shown in Fig. 6a. It was found that, although the GO and GRGO suspensions were biocompatible, the HRGO suspension indicated a cytotoxic property against the prostate cancer cell. It was found that by removing the residual hydrazine of the suspension through filtration and then adjusting the pH of the final suspension to ~7, a nearly biocompatible but aggregated reduced GO suspension was obtained. Therefore, the cytotoxicity of the HRGO suspension can be assigned to the residual hydrazine of the suspension (as known as a toxic material), high pH (>7) of the suspension and/or the cytotoxicity of the non-aggregated reduced GO sheets with extremely sharp edges, as previously reported elsewhere.[17] Strong cytotoxicity of the oxidized SWCNTs and partial cytotoxicity of the oxidized MWCNTs against the prostate cancer cells were also observed, in consistency with some previous reports for cytotoxicity of these carbon-based nanomaterials against various human and animal cells[53–56] and bacteria.[57–59] In contrast to these toxic carbon-based nanomaterial suspensions, the GRGO-Fe showed a biocompatible property which can be assigned to the biocompatible pH of the suspension (~7), the absence of any residual toxic agents required in synthesis of the non-aggregated reduced GO sheets, and/or the steric effect of gluconate ions attached on the reduced sheets prevented effective direct contact interaction of the sheets with wall membrane of the cells. Although the GRGO-Fe, the HRGO and the functionalized SWCNT suspensions exhibited nearly the same efficiencies for the photothermal therapy, the biocompatible property of the GRGO-Fe indicates its more effective performance in the photothermal therapy than the performance of the cytotoxic HRGO and SWCNT suspensions (because some portion of the cell destruction can be assigned to the cytotoxic property of the carbon materials, not to the photothermal therapy). Since the level of reduction of the GRGO-Fe and HRGO is the same (see Table 1), the better performance of the GRGO-Fe than the HRGO can be assigned to lower aggregation of the reduced sheets in the GRGO-Fe (as shown by Raman), providing more effective surface area for further NIR absorption and better heat transfer to the cells. Therefore, the GRGO-Fe can be proposed as a biocompatible graphene-based nanomaterial for efficient photothermal therapy of cancer cells.

Since the cell death following exposure of carbon nanomaterials to NIR radiation can be assigned to thermal disintegration, temperatures of the different solutions (including the solutions containing GO, GRGO-Fe, HRGO and a control sample without any carbon nanomaterials) were measured, as shown in Fig. 6b. The control sample (a solution without any carbon nanomaterials) was transparent to the NIR irradiation and so negligible heating was detected. Similarly, the transparency of the GO solution resulted in only a little heating of the solution after 2 min NIR irradiation, as can be seen in Fig. 6b. However, the NIR irradiation of the aqueous solutions containing GRGO-Fe, HRGO with GO concentration of 0.1 mg mL^{-1} for 2 min caused heating of the solution to temperatures of about 64 and 70 °C, respectively. For longer irradiations, boiling of the solutions was also observed. These results indicated that the energy absorbed by the photo-stimulated graphene-based nanomaterials can quickly transfer to molecular vibration energies and consequently heating. It should be noted that the biocompatible GRGO-Fe solution with a slightly lower temperature (64 °C) was more efficient than the toxic HRGO with a higher temperature (70 °C) in photothermal destruction of the cancer cells. This means that the photo-stimulated GRGO-Fe showed a better heat transfer to the cancer cells (rather than the solution), and consequently, a further increase in local temperature of the cells (as compared to the measured temperature of the solution) than the photo-stimulated HRGO. The better heat transfer of the GRGO-Fe than the HRGO can be assigned to higher content of single-sheets of reduced graphene in the former, as also found by analysis of the Raman spectra.

The cell viability of the cancer cells was studied by using a bright-field inverted microscopy method (Fig. 7) and MTT test (Fig. 8a), after photothermal therapy by the GRGO-Fe at various NIR irradiation times. For the microscopy method, the cells were stained with Trypan Blue to find the extent of the cell death. The circular regions in Fig. 7 represent the positions of laser spots. The radius of the laser spot was ~5 mm, as measured by using a photosensitive paper. A control sample was also incubated without any graphene-based nanomaterials (see the right column in Fig. 7). The left column in Fig. 7 shows that dead cells appeared after 30 s photothermal therapy. By increasing the irradiation time to 120 s, most of the cancer cells, especially located at the center of the circular area, were dead. The same results were obtained by MTT test as shown in Fig. 8a. The control samples showed no considerable dead cells even after 120 s NIR irradiation (see Fig. 7 and 8a). Fig. 7 also shows that no considerable dead cells were distinguishable for the cells outside of the laser spot, very similar to the control samples. This means that the GRGO-Fe sheets themselves showed no significant cytotoxic property. The MTT test also indicated that the transparent GO sheets were not so effective in the photothermal therapy (see Fig. 8a). This presents the effect of the effective deoxygenation of GO through reduction by glucose in the presence of Fe catalyst on the photothermal therapy of the cells.

Using the MTT test, we also studied the effect of various concentrations of GRGO-Fe on the photothermal therapy of the cancer cells for different NIR irradiation times, as shown in Fig. 8b. It was found that for the high concentration of 1 mg mL^{-1}, only 0.5 min irradiation time was required for photothermal destruction of all of the cancer cells. On the other hand, the lowest concentration required for complete photothermal lysis of the cancer cells within the long irradiation time of 12 min was 0.05 mg mL^{-1}. To have some comparison, it is worth noting that Yang *et al.*[11] could completely eliminate the tumors of mice through intravenous injection of 2 mg mL^{-1} nGO-PEG after 24 h NIR irradiation with power density of 2 W cm^{-2}. This group

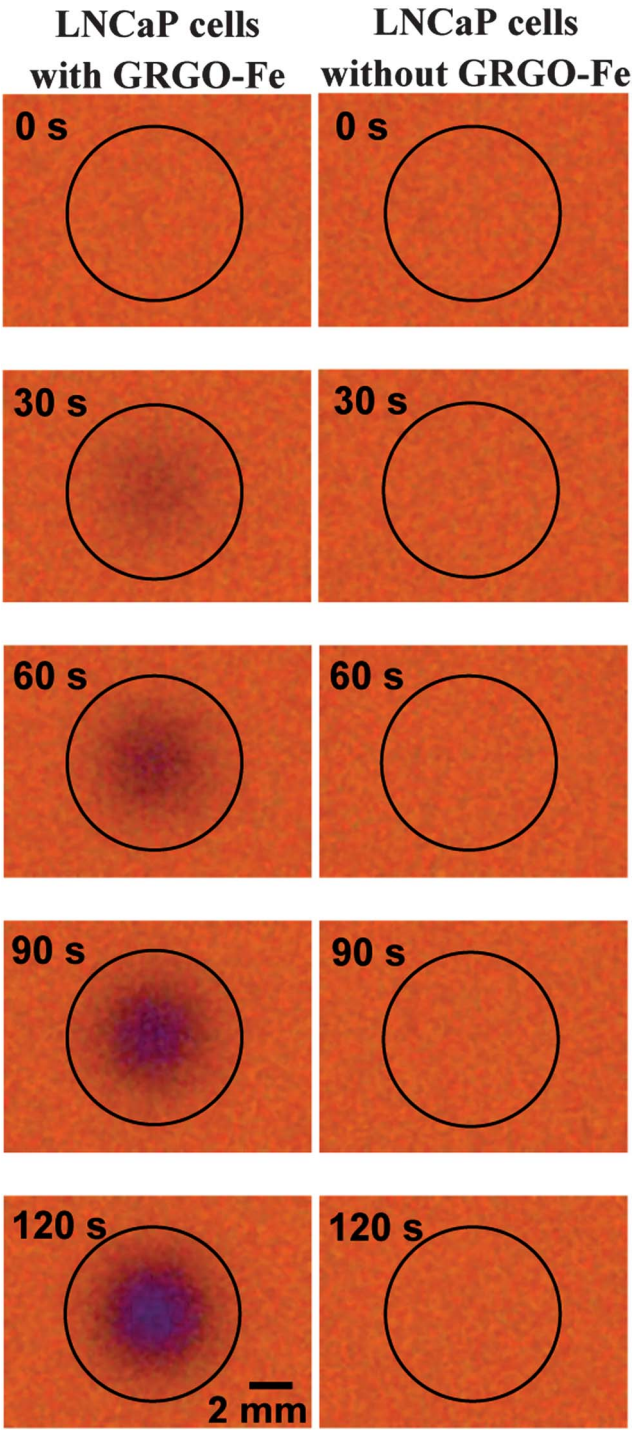

Fig. 7 Optical images of photothermal destruction of LNCaP prostate cancer cells incubated with 0.05 mg mL^{-1} GRGO-Fe nanosheets at various times of NIR irradiation with power density of 7.5 W cm^{-2}. The circles show position of the laser spot.

using nRGO-PEG (2 mg mL^{-1}) obtained a complete tumor elimination by using ultra-low power density of 0.15 W cm^{-2} for 5 min.[12] Robinson *et al.*[13] could photothermally destroy 80% of cancer cells *in vitro* by using a low-concentration (6.6 mg L^{-1}) of nRGO-PEG after 20 min NIR irradiation with power density of 15.3 W cm^{-2}. Therefore, the efficiency of the GRGO-Fe sheets

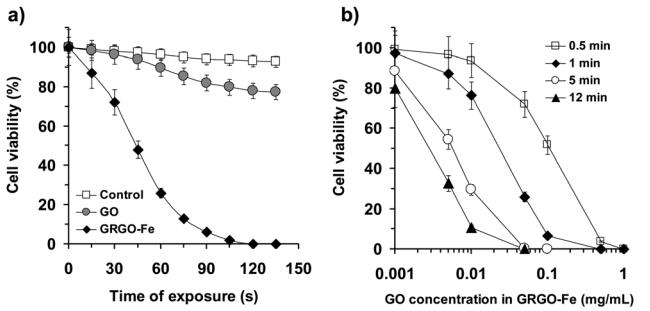

Fig. 8 Cell viability of LNCaP prostate cancer cells *versus* (a) NIR irradiation exposure time after incubation with the GO and the GRGO-Fe (with GO concentration of 0.05 mg mL^{-1}) as compared to a control sample (cancer cells without the graphene materials) and (b) GO concentration in the GRGO-Fe at some various NIR irradiation exposure times.

in photothermal nanotherapy is comparable with the efficiencies that have been reported so far.

4. Conclusions

Biocompatible reduced graphene oxide sheets with suitable water-solubility were obtained through functionalization of the reduced sheets by gluconate ions produced during the reduction by glucose in the presence of Fe catalyst, without any PEGylation (as a common functionalization method). In addition, for the first time, the GRGO-Fe was utilized as a biocompatible graphene-based nanomaterial suspension for a highly efficient NIR photothermal therapy of LNCaP prostate cancer cells *in vitro*. It was found that the GRGO-Fe with a high (low) concentration of 1 (0.05) mg mL^{-1} requires only 0.5 (12) min for complete destruction of the cancer cells under irradiation of an 808 nm laser source with power density of 7.5 W cm^{-2}. Although the photothermal therapy using the HRGO, SWCNT and MWCNT suspensions could show similar efficiencies, these suspensions indicated some cytotoxic effects. These results indicated that the GRGO-Fe can be proposed as one of the promising biocompatible nanomaterials for application in effective NIR photothermal nanotherapy of cancer cells.

Acknowledgements

O. Akhavan would like to thank the Research Council of Sharif University of Technology and also Iran Nanotechnology Initiative Council for financial support of the work.

References

1 A. Coates, S. Abraham, S. B. Kaye, T. Sowerbutts, C. Frewin, R. M. Fox and H. Tattersall, On the receiving end-patient perception of the side-effects of cancer chemotherapy, *Eur. J. Cancer Clin. Oncol.*, 1983, **19**, 203–208.
2 B. Zachariah, L. Balducci, G. V. Venkattaramanabalaji, L. Casey, H. M. Greenberg and J. A. DelRegato, Radiotherapy for cancer patients aged 80 and older: a study of effectiveness and side effects, *Int. J. Radiat. Oncol., Biol., Phys.*, 1997, **39**, 1125–1129.
3 M. G. Michael, F. Tito and E. B. Susan, Multidrug resistance in cancer: role of ATP-dependent transporters, *Nat. Rev. Cancer*, 2002, **2**, 48–58.

4 G. Szakács, J. K. Paterson, J. A. Ludwig, C. Booth-Genthe and M. M. Gottesman, Targeting multidrug resistance in cancer, *Nat. Rev. Drug Discovery*, 2006, **5**, 219–234.
5 H. K. Moon, S. H. Lee and H. C. Choi, *In vivo* near-infrared mediated tumor destruction by photothermal effect of carbon nanotubes, *ACS Nano*, 2009, **3**, 3707–3713.
6 F. Zhou, D. Xing, Z. Ou and B. Wu, Cancer cell photothermal therapy in near infrared region by using single walled carbon nanotubes, *J. Biomed. Opt.*, 2009, **142**, 021009.
7 S. Ghosh, S. Dutta, E. Gomes, D. Carroll, R. D'Agostino, Jr, J. Olson and W. H. Gmeiner, Increased heating efficiency and selective thermal ablation of malignant tissue with DNA-encased multiwalled carbon nanotubes, *ACS Nano*, 2009, **3**, 2667–2673.
8 O. Akhavan, E. Ghaderi and R. Rahighi, Towards single-DNA electrochemical biosensing by graphene nanowalls, *ACS Nano*, 2012, **6**, 2904–2916.
9 D. B. Leper, Molecular and cellular mechanisms of hyperthermia alone or combined with other modalities, in *Hyperthermic Oncology*, ed. J. Overgaard, Taylor and Francis, London, 1984, pp. 9–40.
10 Y. K. Koh, M. Bae, D. G. Cahill and E. Pop, Heat conduction across monolayer and few-layer graphenes, *Nano Lett.*, 2010, **10**, 4363–4368.
11 K. Yang, S. Zhang, G. Zhang, X. Sun, S. T. Lee and Z. Liu, Graphene in mice: ultrahigh *in vivo* tumor uptake and efficient photothermal therapy, *Nano Lett.*, 2010, **10**, 3318–3323.
12 K. Yang, J. Wan, S. Zhang, B. Tian, Y. Zhang and Z. Liu, The influence of surface chemistry and size of nanoscale graphene oxide on photothermal therapy of cancer using ultra-low laser power, *Biomaterials*, 2011, **33**, 2206–2214.
13 J. T. Robinson, S. M. Tabakman, Y. Liang, H. Wang, H. Sanchez Casalongue, D. Vinh and H. Dai, Ultrasmall reduced graphene oxide with high near-infrared absorbance for photothermal therapy, *J. Am. Chem. Soc.*, 2011, **133**, 6825–6831.
14 W. Zhang, Z. Guo, D. Huang, Z. Liu, X. Guo and H. Zhong, Synergistic effect of chemo-photothermal therapy using PEGylated graphene oxide, *Biomaterials*, 2011, **32**, 8555–8561.
15 Z. M. Markovic, L. M. Harhaji-Trajkovic, B. M. Todorovic-Markovic, D. P. Kepic, K. M. Arsikin, S. P. Jovanovic, A. C. Pantovic, M. D. Dramicanin and V. S. Trajkovic, *In vitro* comparison of the photothermal anticancer activity of graphene nanoparticles and carbon nanotubes, *Biomaterials*, 2011, **32**, 1121–1129.
16 S. Park, N. Mohanty, J. W. Suk, A. Nagaraja, J. An, R. D. Piner, W. Cai, D. R. Dreyer, V. Berry and R. S. Ruoff, Biocompatible, robust free-standing paper composed of a TWEEN/graphene composite, *Adv. Mater.*, 2010, **22**, 1736–1740.
17 O. Akhavan and E. Ghaderi, Toxicity of graphene and graphene oxide nanowalls against bacteria, *ACS Nano*, 2010, **4**, 5731–5736.
18 Y. Zhang, S. F. Ali, E. Dervishi, Y. Xu, Z. Li, D. Casciano and A. S. Biris, Cytotoxicity effects of graphene and single-wall carbon nanotubes in neural phaeochromocytoma-derived PC12 cells, *ACS Nano*, 2010, **4**, 3181–3186.
19 O. Akhavan, E. Ghaderi and A. Esfandiar, Wrapping bacteria by graphene nanosheets for isolation from environment, reactivation by sonication and inactivation by near-infrared irradiation, *J. Phys. Chem. B*, 2011, **115**, 6279–6288.
20 W. Hu, C. Peng, W. Luo, M. Lv, X. Li, D. Li, Q. Huang and C. Fan, Graphene-based antibacterial paper, *ACS Nano*, 2010, **4**, 4317–4323.
21 K. H. Liao, Y. S. Lin, C. W. MacOsko and C. L. Haynes, Cytotoxicity of graphene oxide and graphene in human erythrocytes and skin fibroblasts, *ACS Appl. Mater. Interfaces*, 2011, **3**, 2607–2615.
22 A. Esfandiar, O. Akhavan and A. Irajizad., Melatonin as a powerful bio-antioxidant for reduction of graphene oxide, *J. Mater. Chem.*, 2011, **21**, 10907–10914.
23 J. Gao, F. Liu, Y. Liu, N. Ma, Z. Wang and X. Zhang, Environment-friendly method to produce graphene that employs vitamin C and amino acid, *Chem. Mater.*, 2010, **22**, 2213–2218.
24 C. Zhu, S. Guo, Y. Fang and S. Dong, Reducing sugar: new functional molecules for the green synthesis of graphene nanosheets, *ACS Nano*, 2010, **4**, 2429–2437.
25 O. Akhavan, M. Kalaee, Z. S. Alavi, S. M. A. Ghiasi and A. Esfandiar, Increasing the antioxidant activity of green tea polyphenols in the presence of iron for the reduction of graphene oxide, *Carbon*, 2012, **50**, 3015–3025.
26 O. Akhavan and E. Ghaderi, *Escherichia coli* bacteria reduce graphene oxide to bactericidal graphene in a self-limiting manner, *Carbon*, 2010, **50**, 1853–1860.
27 E. C. Salas, Z. Sun, A. Lüttge and J. M. Tour, Reduction of graphene oxide *via* bacterial respiration, *ACS Nano*, 2010, **4**, 4852–4856.
28 O. Akhavan, R. Azimirad, S. Safa and M. M. Larijani, Visible light photo-induced antibacterial activity of CNT-doped TiO_2 thin films with various CNT contents, *J. Mater. Chem.*, 2010, **20**, 7386–7392.
29 O. Akhavan, R. Azimirad and S. Safa, Functionalized carbon nanotubes in ZnO thin films for photoinactivation of bacteria, *Mater. Chem. Phys.*, 2011, **130**, 598–602.
30 H. C. Schniepp, J. L. Li, M. J. McAllister, H. Sai, M. Herrera-Alonso, D. H. Adamson, R. K. Prud'homme, R. Car, D. A. Saville and I. A. Aksay, Functionalized single graphene sheets derived from splitting graphite oxide, *J. Phys. Chem. B*, 2006, **110**, 8535–8539.
31 O. Akhavan, The effect of heat treatment on formation of graphene thin films from graphene oxide nanosheets, *Carbon*, 2010, **48**, 509–519.
32 M. J. McAllister, J. L. Li, D. H. Adamson, H. C. Schniepp, A. A. Abdala, J. Liu, M. Herrera-Alonso, D. L. Milius, R. Car, R. K. Prud'homme and I. A. Aksay, Single sheet functionalized graphene by oxidation and thermal expansion of graphite, *Chem. Mater.*, 2007, **19**, 4396–4404.
33 Q. Su, S. Pang, V. Alijani, C. Li, X. Feng and K. Müullen, Composites of graphene with large aromatic molecules, *Adv. Mater.*, 2009, **21**, 3191–3195.
34 D. Li, M. B. Muller, S. Gilje, R. B. Kaner and G. G. Wallace, Processable aqueous dispersions of graphene nanosheets, *Nat. Nanotechnol.*, 2008, **3**, 101–105.
35 F. Liu and T. S. Seo, A controllable self-assembly method for large-scale synthesis of graphene sponges and free-standing graphene films, *Adv. Funct. Mater.*, 2010, **20**, 1–7.
36 C. Xu, X. Wang and J. Zhu, Graphene-metal particle nanocomposites, *J. Phys. Chem. C*, 2008, **112**, 19841–19845.
37 A. C. Ferrari and J. Robertson, Interpretation of Raman spectra of disordered and amorphous carbon, *Phys. Rev. B: Condens. Matter*, 2000, **61**, 14095–14107.
38 S. Stankovich, D. A. Dikin, R. D. Piner, K. A. Kohlhaas, A. Kleinhammes, Y. Jia, S. T. Nguyen and R. S. Ruoff, Synthesis of graphene-based nanosheets *via* chemical reduction of exfoliated graphite oxide, *Carbon*, 2007, **45**, 1558–1565.
39 A. C. Ferrari, J. C. Meyer, V. Scardaci, C. Casiraghi, M. Lazzeri, F. Mauri, S. Piscanec, D. Jiang, K. S. Novoselov, S. Roth and A. K. Geim, Raman spectrum of graphene and graphene layers, *Phys. Rev. Lett.*, 2006, **97**, 187401–187405.
40 C. Thomsen and S. Reich, Double resonant Raman scattering in graphite, *Phys. Rev. Lett.*, 2000, **85**, 5214–5217.
41 L. M. Malard, M. A. Pimenta, G. Dresselhaus and M. S. Dresselhaus, Raman spectroscopy in graphene, *Phys. Rep.*, 2009, **473**, 51–87.
42 D. Graf, F. Molitor, K. Ensslin, C. Stampfer, A. Jungen, C. Hierold and L. Wirtz, Spatially resolved Raman spectroscopy of single- and few-layer graphene, *Nano Lett.*, 2007, **7**, 238–242.
43 O. Akhavan and E. Ghaderi, Photocatalytic reduction of graphene oxide nanosheets on TiO_2 thin film for photoinactivation of bacteria in solar light irradiation, *J. Phys. Chem. C*, 2009, **113**, 20214–20220.
44 G. Williams, B. Seger and P. V. Kamat, TiO_2-graphene nanocomposites. UV-assisted photocatalytic reduction of graphene oxide, *ACS Nano*, 2008, **2**, 1487–1491.
45 O. Akhavan, M. Abdolahad, A. Esfandiar and M. Mohatashamifar, Photodegradation of graphene oxide sheets by TiO_2 nanoparticles after a photocatalytic reduction, *J. Phys. Chem. C*, 2010, **114**, 12955–12959.
46 O. Akhavan, Graphene nanomesh by ZnO nanorod photocatalysts, *ACS Nano*, 2010, **4**, 4174–4180.
47 G. Williams and P. V. Kamat, Graphene-semiconductor nanocomposites: excited-state interactions between ZnO nanoparticles and graphene oxide, *Langmuir*, 2009, **25**, 13869–13873.
48 O. Akhavan, Photocatalytic reduction of graphene oxides hybridized by ZnO nanoparticles in ethanol, *Carbon*, 2011, **49**, 11–18.
49 Y. H. Ng, A. Iwase, N. J. Bell, A. Kudo and R. Amal, Semiconductor/reduced graphene oxide nanocomposites derived from photocatalytic reactions, *Catal. Today*, 2011, **164**, 353–357.

50 O. Akhavan, M. Choobtashani and E. Ghaderi, Protein degradation and RNA efflux of viruses photocatalyzed by graphene-tungsten oxide composite under visible light irradiation, *J. Phys. Chem. C*, 2012, **116**, 9653–9659.
51 Q. Zeng, J. S. Cheng, X. F. Liu, H. T. Bai and J. H. Jiang, Palladium nanoparticle/chitosan-grafted graphene nanocomposites for construction of a glucose biosensor, *Biosens. Bioelectron.*, 2011, **26**, 3456–3463.
52 R. B. Robey and N. Hay, Mitochondrial hexokinases, novel mediators of the antiapoptotic effects of growth factors and Akt, *Oncogene*, 2006, **25**, 4683–4696.
53 A. A. Shvedova, V. Castranova, E. R. Kisin, D. Schwegler-Berry, A. R. Murray, V. Z. Gandelsman, A. Maynard and P. Baron, Exposure to carbon nanotube material: assessment of nanotube cytotoxicity using human Keratinocyte cells, *J. Toxicol. Environ. Health, Part A*, 2003, **66**, 1909–1926.
54 S. K. Manna, S. Sarkar, J. Barr, K. Wise, E. V. Barrera, O. Jejelowo, A. C. Rice-Ficht and G. T. Ramesh, Single-walled carbon nanotube induces oxidative stress and activates nuclear transcription factor-κB in human Keratinocytes, *Nano Lett.*, 2005, **5**, 1676–1684.
55 C. W. Lam, J. T. James, R. McCluskey and R. L. Hunter, Pulmonary toxicity of single-wall carbon nanotubes in mice 7 and 90 days after intractracheal instillation, *Toxicol. Sci.*, 2004, **77**, 126–134.
56 X. Chen, U. C. Tam, J. L. Czlapinski, G. S. Lee, D. Rabuka, A. Zettl and C. R. Bertozzi, Interfacing carbon nanotubes with living cells, *J. Am. Chem. Soc.*, 2006, **128**, 6292–6293.
57 S. Kang, M. Pinault, L. Pfefferle and M. Elimelech, Single-walled carbon nanotubes exhibit strong antimicrobial activity, *Langmuir*, 2007, **23**, 8670–8673.
58 S. Kang, M. Herzberg, D. F. Rodrigues and M. Elimelech, Antibacterial effects of carbon nanotubes: size does matter!, *Langmuir*, 2008, **24**, 6409–6413.
59 O. Akhavan, M. Abdolahad, Y. Abdi and S. Mohajerzadeh, Silver nanoparticles within vertically aligned multi-wall carbon nanotubes with open tips for antibacterial purposes, *J. Mater. Chem.*, 2011, **21**, 387–393.